Materials Advances

ROYAL SOCIETY OF CHEMISTRY

PAPER

View Article Online
View Journal | View Issue

Cite this: *Mater. Adv.*, 2024, 5, 6605

Porous ceria materials for efficient direct conversion of carbon dioxide and methanol to dimethyl carbonate†

Zhuxian Yang,[a] Justin Tay Zheng,[b] Xinhuan Lu,[c] Monica Mengdie Lin,[b] Dongming Cai,[d] Yankun Wang,[a] Wen-Yueh Yu, *[b] Yanqiu Zhu [a] and Yongde Xia *[a]

Ceria (CeO_2) is widely considered as a superior catalytic material for the direct conversion of carbon dioxide (CO_2) and methanol into dimethyl carbonate (DMC). Developing porous structures is a versatile way to increase the surface area, to create defects, and to improve the mass transfer of the resulting materials, consequently enhancing their catalytic performance. However, most of the reported preparation methods of porous CeO_2 involve complex hydrothermal (100–120 °C) or refluxing (95–140 °C) processes followed by calcination at temperatures of 500–650 °C. In this work, we report a simple and low temperature approach to prepare porous CeO_2, which involves mixing the raw materials at room temperature, followed by drying and then calcining at 450 °C. A DMC formation rate of 14.8 mmol g^{-1} h^{-1} is achieved for one of the obtained porous CeO_2, which is much higher than those of the most reported CeO_2 (0.51–11 mmol g^{-1} h^{-1}). Further studies show that the DMC formation rate has a positive link to the parameters following the order: the CO_2 uptake amount at 25 °C, the amount of weak acidity, the Ce^{3+} concentration, the amount of weak basicity, and the BET surface area of the CeO_2 catalysts in this study. In addition, there seems to be an optimum oxygen vacancy concentration of the CeO_2 samples for the DMC formation rate. This study provides a simple strategy for the preparation of a porous CeO_2 material as a highly efficient catalyst for the catalytic conversion of CO_2, which can not only mitigate the greenhouse gas CO_2, but also turn it into value-added and versatile chemical DMC.

Received 18th June 2024,
Accepted 15th July 2024

DOI: 10.1039/d4ma00629a

rsc.li/materials-advances

1. Introduction

Dimethyl carbonate (DMC) exhibits a number of promising properties including low toxicity, high oxygen content (53%), low viscosity, good dissolving ability, and a high-octane number (105).[1,2] DMC can be used as a green solvent and a fuel additive.[3,4] Thanks to its multiple functionalities, DMC can also be used as a versatile reagent for methylation, carbonylation, and methoxycarbonylation.[5] Recently the market demand for DMC has been increasing significantly because of its widespread applications.[6]

There are a number of methods for DMC preparation, and some of them have been industrialised,[6–8] while others are under study.[9–12] There are, however, some issues with the industrialised processes, such as the involvement of hypertoxic phosgene, high cost, explosion risk, *etc.*[6,13] Among the various methods that have been studied for DMC production, the direct synthesis of DMC from CO_2 and methanol is attractive because it does not involve any toxicants, moreover it can turn the greenhouse gas CO_2 into DMC,[11,14–21] a value-added and versatile product. This method is based on the following equation:

$$CO_2 + 2CH_3OH \rightleftharpoons (CH_3O)_2CO + H_2O$$

The major issues with this method are the high stability of CO_2 and the low equilibrium constant of the reaction, leading to a low DMC yield. Catalysts, high CO_2 pressure/temperature and dehydrating agents have been employed to address these issues.[4,6,11,19,22–24] Applying dehydrating agents to remove the *in situ* produced water can shift the equilibrium to the product

[a] *Department of Engineering, Faculty of Environment, Science and Economy, University of Exeter, Exeter, EX4 4QF, UK. E-mail: y.xia@exeter.ac.uk*
[b] *Department of Chemical Engineering, National Taiwan University, No. 1, Sec. 4, Roosevelt Rd, Taipei, 106335, Taiwan. E-mail: wenyueh@ntu.edu.tw*
[c] *School of Chemical Engineering, Hubei University, 368 Youyi Dadao, Wuchang Qu, Wuhan, Hubei Province, 430062, P. R. China*
[d] *Hubei Key Laboratory of Energy Storage and Power Battery, School of Mathematics, Physics and Optoelectronics Engineering, Hubei University of Automotive Technology, Shiyan, 442002, P. R. China*

† Electronic supplementary information (ESI) available. See DOI: https://doi.org/10.1039/d4ma00629a

side and consequently increase the DMC yield.[22,23,25–30] Regarding catalysts, a large number of catalysts have been investigated for direct DMC synthesis including, CeO_2,[17–19,31–33] ZrO_2,[34–37] V_2O_5,[38] Y_2O_3,[39] *etc.* Among them, CeO_2 based catalysts have shown superior catalytic performance and attracted considerable attention.[31–33,40–42]

Yoshida *et al.* first studied CeO_2 prepared by calcining commercial CeO_2 as the catalyst for direct synthesis of DMC from CO_2 and methanol.[11] Ever since this report, a number of CeO_2 based catalysts prepared *via* various synthesis strategies have been evaluated for the direct synthesis of DMC, including the hydrothermal method,[15,20,43–45] solvothermal method,[46] precipitation method,[23,32,40,41,47–49] templating method,[50] refluxing method,[19] *etc.* These various strategies resulted in CeO_2 based catalysts with different properties and accordingly significantly different catalytic performance. It has been found that the specific surface area,[11,30,47] morphologies,[15,44,51,52] acid–base properties,[33,45,46,53–56] oxygen-vacancies,[16,19,21,30,46,57,58] surface Ce^{3+} content[19,21,58] or Ce^{4+} content[32,59] of CeO_2 based catalysts can affect their catalytic performance.

Developing porous catalysts is an efficient approach to increase the surface area, to create defects, and to improve the mass transfer of the resulting catalysts, and consequently enhance the catalytic performance.[19,30,60–62] Porous CeO_2 can be prepared by a polyol method,[63] hydrothermal method,[20,60,62] solvent evaporation-induced self-assembly method,[30] sol method,[64] hard template method,[61] reflux process,[19] soft-to-hard consecutive template method,[65] *etc.* Although these strategies can produce porous CeO_2 with a surface area of *ca.* 100–220 $m^2\ g^{-1}$, most of them are tedious and involve complex steps. It is therefore desirable to develop a simple synthesis approach to prepare highly porous CeO_2 catalysts for the direct preparation of DMC from CO_2 and methanol.

In this study, we report the preparation of porous CeO_2 by a simple method at lower temperature, which involves mixing the raw materials at room temperature, followed by drying at 70 °C and then 100 °C, and finally annealing at 450 °C. The resulting CeO_2 was characterised by N_2 adsorption analysis, CO_2 adsorption analysis, XRD, Raman spectroscopy, XPS, SEM, TEM, temperature-programmed desorption of NH_3 (NH_3-TPD) and CO_2 (CO_2-TPD), and further evaluated for the direct synthesis of DMC from CO_2 and methanol without applying a dehydrating agent. A high DMC formation rate of 14.8 mmol g^{-1} h^{-1} has been achieved for the CeO_2 sample calcined at 450 °C with a heating rate of 1.4 °C min^{-1}, which is much higher than the majority of the reported CeO_2 catalysts. This sample was further studied by *in situ* diffuse reflectance infrared Fourier transform spectroscopy (DRIFTS) for the DMC formation mechanism. The effect of the BET surface area (S_{BET}), the CO_2 uptake amount at 25 °C, the weak acidity, the weak basicity, the Raman peak intensity ratio of $I_D/I_{F_{2g}}$, the XPS Ce^{3+} concentration (Ce^{3+}%), and the XPS oxygen vacancy concentration (O_V%) of the CeO_2 samples prepared under different conditions on the DMC formation rate has been investigated.

2. Materials and methods

2.1. Materials

Pluronic F-127, phloroglucinol ($C_6H_6O_3$), cerium(III) nitrate hexahydrate ($Ce(NO_3)_3{\cdot}6H_2O$), nitric acid (70%) (HNO_3) and formaldehyde (37%) (HCHO) were purchased from Merck. Absolute ethanol (C_2H_5OH) was purchased from Fisher Scientific.

2.2. Preparation of porous CeO_2

The CeO_2 precursor was prepared following a slightly modified procedure reported by Lee *et al.*[65] In brief, 0.3 mmol Pluronic F-127 ($C_7H_{16}O_4$), 10 mmol phloroglucinol ($C_6H_6O_3$), and 10 mmol $Ce(NO_3)_3{\cdot}6H_2O$ were dissolved in 25 mL of ethanol, followed by adding 1.1 mmol HNO_3 (70%) under vigorous stirring for 30 min, and then 15 mmol HCHO was added under stirring for 2 h. The resulting mixture was dried in an oven at 70 °C for 24 h, and then at 100 °C for 24 h to produce the CeO_2 precursor.

The CeO_2 precursor was calcined to generate porous CeO_2 *via* two different methods, *i.e.*, two-step calcination and one-step calcination. In the two-step calcination process, the CeO_2 precursor was heated in argon at 800 °C with a ramp rate of 5 °C min^{-1} for 3 h, followed by calcination in air at 450 °C with a ramp rate of 1.4 °C min^{-1} for 3 h to remove carbon, and the obtained CeO_2 was named Ar800-5.0_Air450-1.4. In the one-step calcination process, the CeO_2 precursor was directly calcined in air at 400 or 450 °C with a heating rate of 1.4 °C min^{-1} for 3 h to generate CeO_2 named Air400-1.4 and Air450-1.4 respectively; while the CeO_2 precursor underwent direct calcination in air at 450 °C with a heating rate of 5 °C min^{-1} for 3 h resulting in CeO_2 named Air450-5.0.

2.3. Sample characterisation

N_2 gas sorption analysis was measured with a Quantachrome Autosorb-iQ gas analyser using a conventional volumetric technique at −196 °C. Samples were outgassed under vacuum at 200 °C for 6 h prior to analysis. The surface area was calculated using the Brunauer–Emmett–Teller (BET) method using adsorption data in the partial pressure (P/P_0) range of 0.05–0.2. The pore size distribution was calculated with the DFT model with adsorption data. CO_2 gas sorption analysis was performed in the same way as N_2 gas sorption analysis except that the analysis temperature was 25 °C. X-ray diffraction (XRD) patterns were obtained with a Bruker D8 Advance X-ray diffractometer with a Cu Kα X-ray source (λ = 0.15418 nm) at 40 kV and 40 mA. X-ray photoelectron spectroscopy (XPS) analysis was performed with a Kratos Axis Ultra system with a monochromated Al Kr X-ray source operated at an emission current of 10 mA and an anode potential of 15 kV. The XPS spectra were deconvoluted with CasaXPS software. Raman spectroscopy measurement was carried out with a Renishaw inVia Qontor with a 532 nm laser.

In situ FT-IR spectra were recorded with an infrared spectrometer (Thermo Scientific Nicolet iS50) equipped with a mercury–cadmium–telluride (MCT) detector and a diffuse reflectance infrared Fourier transform spectroscopy (DRIFTS) chamber

(Harrick Praying Mantis™ HVC-DRP-5).[19,66–68] The measurements were carried out as follows:[19] the chamber was pre-treated at 200 °C in Ar flow (40 mL min^{-1}) for 20 min. After the chamber was cooled to 140 °C, the methanol in the saturator was introduced to the chamber by Ar flow (40 mL min^{-1}), and the catalyst was purged with Ar flow (40 mL min^{-1}) for 10 min, and then the flow was switched to high-purity CO_2 gas (99.999+%, 40 mL min^{-1}) for 10 min. The DRIFTS spectra were averaged from 16 scans with a resolution of 4 cm^{-1}.

NH_3-TPD was performed with a Quantachrome Chemstar TPX. 100 mg of sample was heated under a helium (He) flow of 30 mL min^{-1} at 300 °C for 40 min to remove surface impurities, followed by cooling. When the temperature was down to 35 °C, a mixture of 5% NH_3/He with a flow rate of 30 mL min^{-1} was introduced into the sample for a period of 30 min for NH_3 adsorption by the sample to take place. Then the sample was purged with nitrogen for 30 min to eliminate the physically adsorbed NH_3 before the desorption of NH_3 took place, which was measured under temperature programming with a heating rate of 10 °C min^{-1} in the range of 50–780 °C. CO_2-TPD was also carried out with a Quantachrome Chemstar TPX. The above procedure used for NH_3-TPD measurement was adopted for CO_2-TPD measurement except that the probe gas NH_3 was replaced by CO_2, and TPD was measured in the range of 50–700 °C.

2.4. Evaluation of catalytic activity for CO_2 conversion

The catalytic activity for CO_2 conversion was measured with a 100-mL Parr reactor without applying a dehydration agent.[19,21,69] 370 mmol methanol and 10 mg of CeO_2 were loaded in a reactor, followed by introducing 5.0 MPa CO_2 at room temperature. The reactor was then heated to 140 °C under stirring and kept at 140 °C for 3 h. Afterwards, the product in the reactor was analysed by a gas chromatograph equipped with a flame ion detector (Agilent 6890N GC-FID) and a capillary column (Zebron ZB-WAX). A pre-determined amount of 1-propanol was applied to the system as the internal standard for quantitative analysis. The DMC formation rate was calculated by dividing the DMC amount obtained at a reaction time of 3 h by the mass of CeO_2 used.

3. Results and discussion

3.1. Structures, textural properties, and morphologies

Fig. 1a shows the XRD patterns of CeO_2 samples prepared under various conditions. Diffraction peaks at 2θ values of 28.4, 32.9, 47.4, 56.3, 59.2, 69.3, 76.7 and 79.0°, corresponding to the (111), (200), (220), (311), (222), (400), (331), and (420) planes of cubic CeO_2 are observed for all of them. The two-step calcined sample (Ar800-5.0_Air450-1.4) exhibits sharper peaks with a much higher

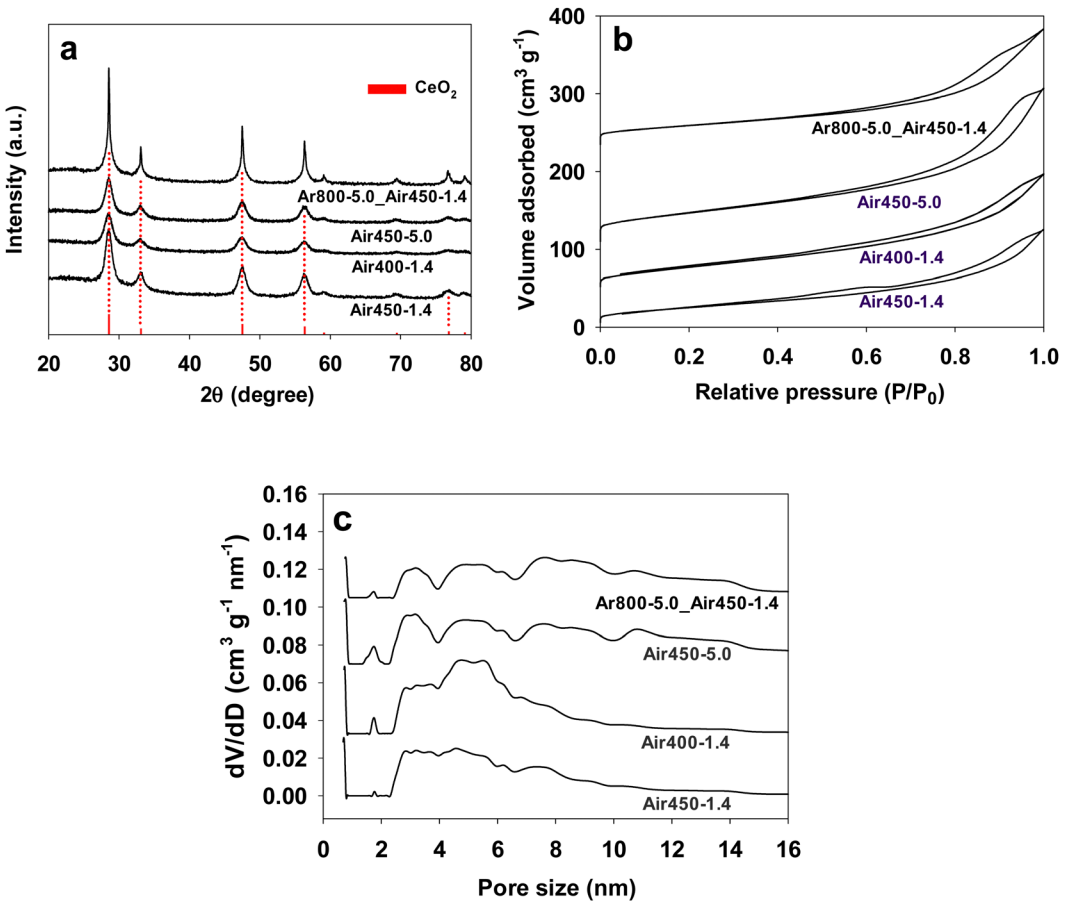

Fig. 1 XRD patterns (a), nitrogen adsorption isotherms (b), and pore size distributions (c) of CeO_2 samples prepared under various calcination conditions which are indicated in their names.

Table 1 Properties and catalytic activity of porous CeO_2 prepared under various conditions

Sample name	Preparation conditions	S_{BET} ($m^2\ g^{-1}$)	Crystal size[a] (nm)	CO_2 uptake[b] (mmol g^{-1})	CO_2 uptake[c] (μmol g^{-1})	NH_3 uptake[d] (μmol g^{-1})	Raman $I_D/I_{F_{2g}}$	XPS Ce^{3+}%	XPS O_V%	DMC formation rate[e] (mmol $g^{-1}\ h^{-1}$)
Ar800-5.0_Air450-1.4	800 °C in Ar + 450 °C in air	89	63.4	0.60	110.6	276.3	0.0081	25.0	38.1	3.3
Air450-1.4	450 °C in air 1.4 °C min^{-1}	104	15.4	1.06	148.4	313.2	0.0080	25.6	31.6	14.8
Air400-1.4	400 °C in air 1.4 °C min^{-1}	127	12.5	0.95	168.2	276.9	0.0073	25.9	28.6	8.9
Air450-5.0	450 °C in air 5 °C min^{-1}	134	13.5	0.88	197.4	334.1	0.0086	24.6	28.2	8.4
Commercial CeO_2 (Strem Chemicals)		60								6.7
CeO_2 octahedra		2			50	50				0.06[15]

[a] Calculated with the Scherrer equation from the (111) XRD peak of CeO_2. [b] Obtained from CO_2 adsorption analysis with a Quantachrome Autosorb-iQ gas analyser at 25 °C. [c] Obtained from CO_2-TPD (100–300 °C). [d] Obtained from NH_3-TPD (100–300 °C). [e] Without applying a dehydration agent.

intensity compared to those samples calcined by one-step, likely due to the high calcination temperature. The crystal sizes estimated with the Scherrer equation (using a Scherrer constant of 0.89 and a λ value of 0.15418 nm) from the (111) XRD peak of CeO_2 are listed in Table 1. The crystal size of Ar800-5.0_Air450-1.4 was estimated to be 63.4 nm, which is much higher than that of the one-step calcined CeO_2 samples (12.5–15.4 nm). This is reasonable given that Ar800-5.0_Air450-1.4 was first calcined at 800 °C in Ar for 3 h before further calcination at 450 °C in air, while the other three samples were only calcined at 450 °C in air for 3 h.

Fig. 1b shows the nitrogen adsorption isotherms of all the CeO_2 samples calcined under various conditions. A hysteresis loop at partial pressure (P/P_0) above 0.4 appears in all the isotherms, suggesting the existence of mesopores in these samples. Fig. 1c reveals that all the samples have multi-mode mesopores, with most pore sizes following in the ranges of 2–4 nm, 4–6 nm and 6–8 nm, whereas samples Ar800-5.0_Air450-1.4 and Air450-5.0 exhibit two extra ranges of 8–10 nm and 10–12 nm. It seems that the heating rate plays a role in the pore size distribution of the resulting samples. The samples obtained from the heating rate of 5.0 °C min^{-1} (Ar800-5.0_Air450-1.4 and Air450-5.0) show one pore size distribution pattern, while the other two samples (Air450-1.4 and Air400-1.4) that resulted from the heating rate of 1.4 °C min^{-1} show another pattern. The pore sizes of these samples are much smaller than the reported values (*e.g.*, 13.8 nm).[19,32,33] This multi-mode pore structure of CeO_2 samples is expected to improve the mass transfer when they are used as catalysts. The BET surface areas of all samples are summarised in Table 1. The one-step calcined samples show a BET surface area of 104–134 $m^2\ g^{-1}$, which is higher than that of the two-step calcined sample (89 $m^2\ g^{-1}$). It is likely that the higher calcination temperature for the two-step calcined sample leads to increased crystallinity of CeO_2 (Fig. 1a) but a decreased surface area. The BET surface area values of the one-step calcined samples (104–134 $m^2\ g^{-1}$) are comparable to the reported ones for CeO_2 prepared by other methods,[19,20,32,60,69] and higher than some reported values (74–88 $m^2\ g^{-1}$),[16,33] but lower than other reported values (170–220 $m^2\ g^{-1}$).[62–64]

The CO_2 isotherms at 25 °C of CeO_2 samples prepared under various calcination conditions are presented in Fig. S1 (ESI†). They all show a hysteresis loop, indicating that the adsorbed CO_2 is not fully desorbed, and sample Air450-1.4 exhibits the largest hysteresis loop, suggesting the strongest interaction between CO_2 and the sample. The calculated physical adsorption capacities of CO_2 are included in Table 1, and sample Air450-1.4 shows the highest CO_2 uptake capacity of 1.06 mmol g^{-1}.

The SEM images of the CeO_2 samples calcined under various conditions are presented in Fig. 2. Fig. 2a–c and g show that all the CeO_2 samples appear to be irregularly shaped lumps with a wide size range of up to around 4 μm × 8 μm, and these lumps are made of tiny particles (Fig. 2d–f and h) regardless of the different calcination conditions. So, calcination has no effect on the morphology of the resulting CeO_2 samples.

The CeO_2 samples obtained *via* one-step calcination (Air450-1.4) and two-step calcination (Ar800-5.0_Air450-1.4) were further observed by TEM as presented in Fig. 3. Fig. 3a and b reveal that both samples are made of irregular tiny particles, and most of which are with estimated sizes in the range of 5–10 nm. In addition, for both samples regardless of the calcination conditions, the (111) plane is the most observed one (Fig. 3c–h) while the (200) plane is occasionally observable (Fig. 3c and d), indicating that the (111) plane could be the active phase for DMC formation.[11,69] These high-resolution TEM image results are in good agreement with the XRD results presented in Fig. 1a. These results indicate that the different calcination conditions do not affect the morphologies and the exposure of the (111) and (200) planes of the resulting CeO_2 samples.

3.2. Acid–base properties

The surface acid–base properties of the samples were evaluated by NH_3-TPD and CO_2-TPD, and the corresponding profiles are shown in Fig. 4. A major broad desorption peak in the temperature range of 100–300 °C appears in the NH_3-TPD profiles for all the CeO_2 samples (Fig. 4a), indicating the presence of weak acidity. However, the intensity of this peak of the one-step calcined samples is higher than that of the two-step calcined

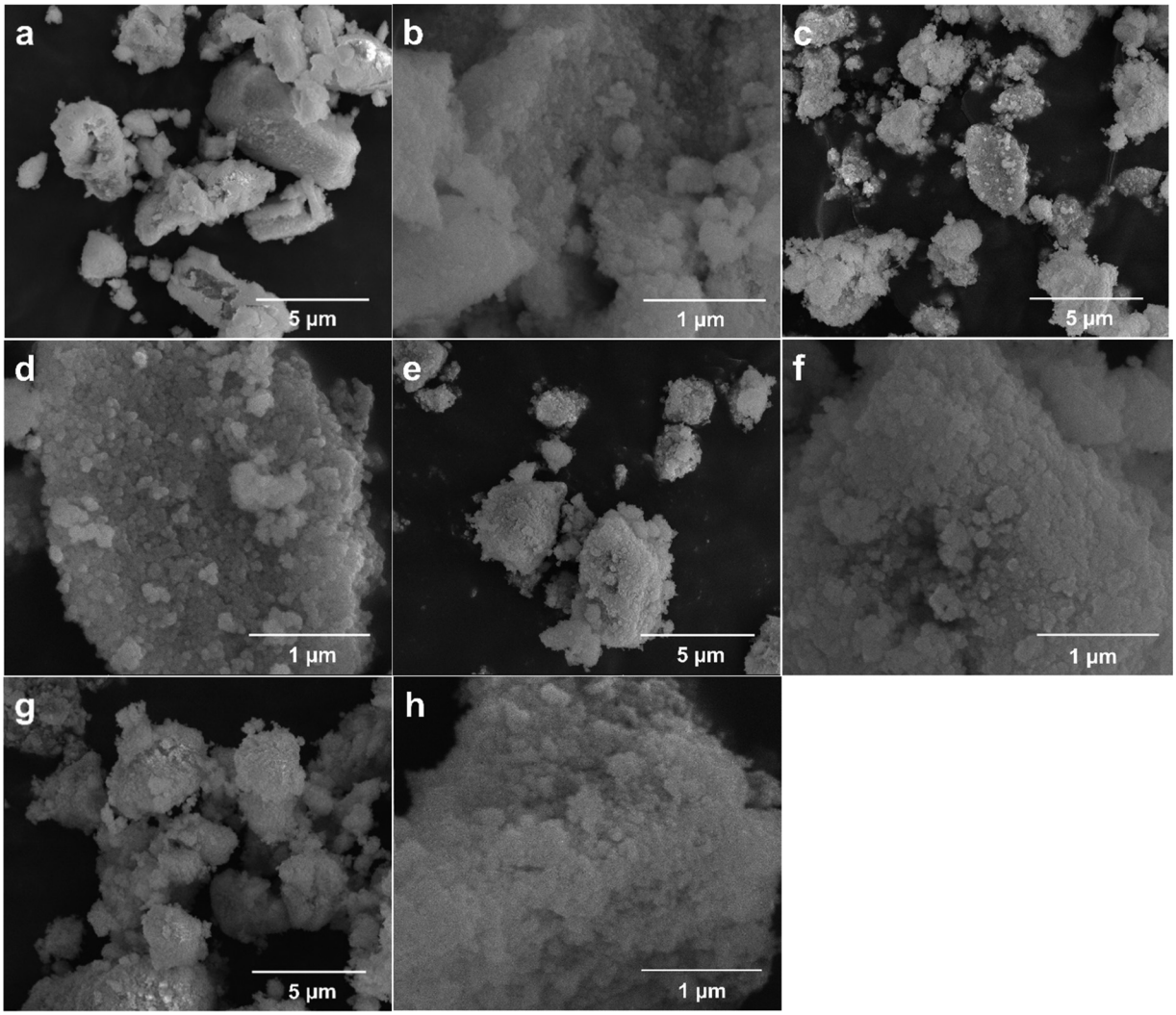

Fig. 2 SEM images of CeO_2 samples calcined under various conditions: Air450-1.4 (a) and (b), Air400-1.4 (c) and (d), Air450-5.0 (e) and (f), and Ar800-5.0_Air450-1.4 (g) and (h).

sample (Ar800-5.0_Air450-1.4), suggesting that the one-step calcined samples exhibit stronger weak acidity. The amount of the weak acidity (the amount of NH_3 adsorbed at 100–300 °C) of all the samples is listed in Table 1. The peak of sample Air450-5.0 is centred at *ca.* 166 °C while that of the other three samples is at *ca.*176 °C. In addition, a weak extra peak at *ca.* 357 °C is observable for the two-step calcined sample (Ar800-5.0_Air450-1.4), implying that two-step calcination results in medium acidity, in addition to weak acidity. Based on the above results, it can be concluded that one-step calcination is superior to two-step calcination in producing stronger weak acidity. This could be one of the reasons that all the one-step calcined samples show a higher DMC formation rate than the two-step calcined sample, as will be discussed later.

Similar to the NH_3-TPD profiles, a major broad CO_2 desorption peak in the temperature range of 100–300 °C can be observed in the CO_2-TPD profiles (Fig. 4b) for all the CeO_2 samples, showing the presence of weak basicity, and the intensity of the CO_2 desorption peak of the one-step calcined samples is also higher than that of the two-step calcined sample (Ar800-5.0_Air450-1.4), suggesting that the one-step calcined samples exhibit stronger weak basicity too. The peak of samples Air450-5.0 and Ar800-5.0_Air450-1.4 is centred at *ca.* 176 °C while that of samples Air450-1.4 and Air400-1.4 is at *ca.* 166 °C. In addition, a weak extra peak at *ca.* 354 °C is observable for the two-step calcined sample Ar800-5.0_Air450-1.4, showing the presence of medium basicity, in addition to weak basicity. According to the above results, it is evident that one-step calcination is superior to two-step calcination in enhancement of both weak acidity and weak basicity of the resulting CeO_2 samples. This enhancement could be one of the reasons that all the one-step calcined samples show higher catalytic activity for the direct conversion of CO_2 into DMC than the two-step calcined sample, as will be discussed later.

3.3. Defects, Ce^{3+}% and O_V%

Raman spectroscopy provides information on molecular vibration and rotation, which can be used to study the detects of

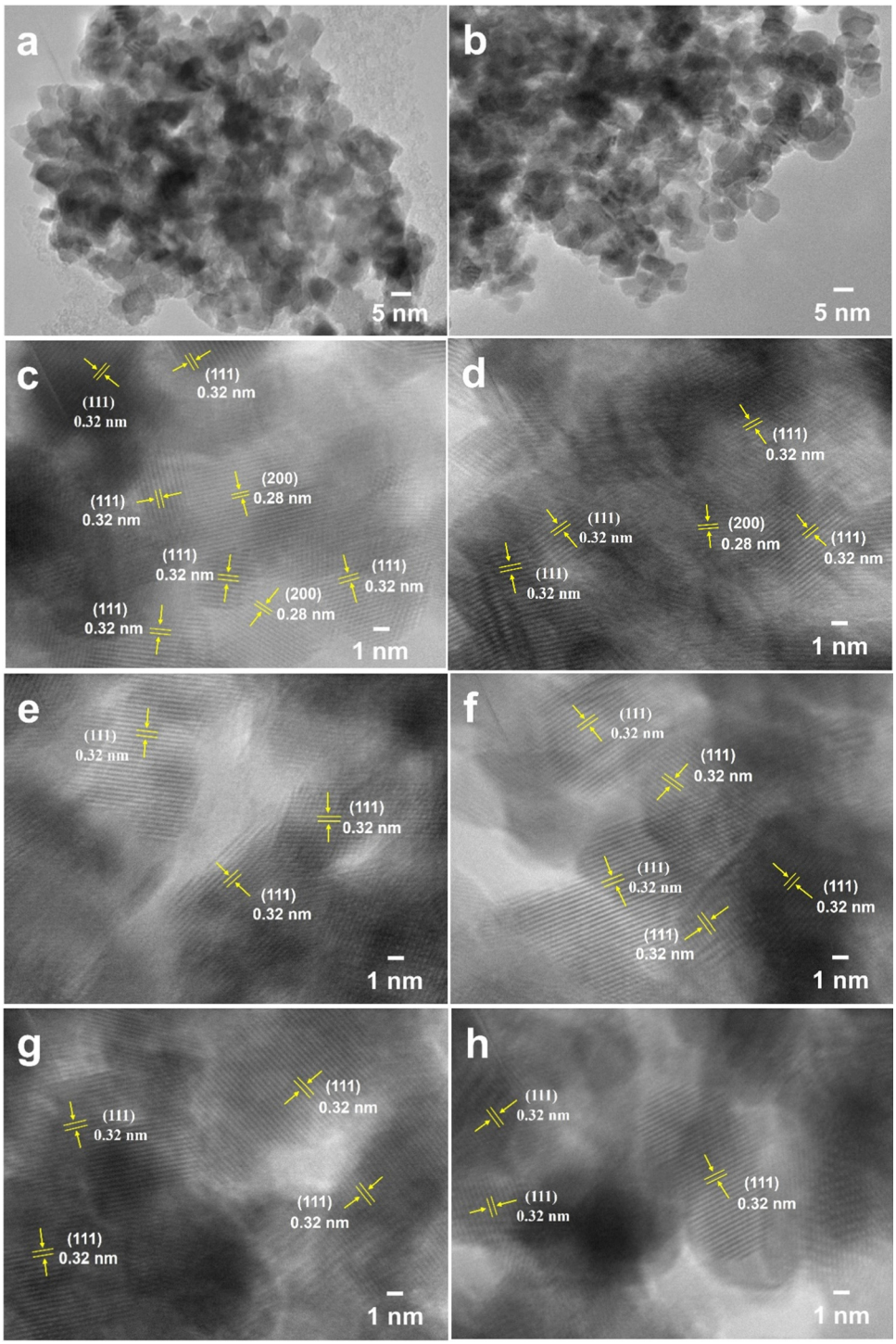

Fig. 3 TEM images of CeO_2 samples Air450-1.4 obtained *via* one-step calcination (a), (c), (e) and (g) and Ar800-5.0_Air450-1.4 obtained *via* two-step calcination (b), (d), (f) and (h).

samples. The Raman spectra (532 nm laser) of CeO_2 samples calcined under various conditions are shown in Fig. 5. All of the samples display Raman peaks at 260.8, 462.8, and 601.6 cm^{-1}, corresponding to the second-order 2TA peak, the first-order F_{2g} peak, and the defect-induced (D) peak, respectively.[70,71] The F_{2g} peak corresponds to the symmetric contraction vibration of Ce–8O in the CeO_2 lattice, which is sensitive to any disorder, doping, or particle-size-induced effects in the lattice caused by heating.[72] It is generally accepted that the intensity ratio of the D peak to the F_{2g} peak ($I_D/I_{F_{2g}}$) is an indicator of the amount of defects of CeO_2-based catalysts.[16,19,73] The intensity ratio ($I_D/I_{F_{2g}}$) values of all the CeO_2 samples have been calculated and

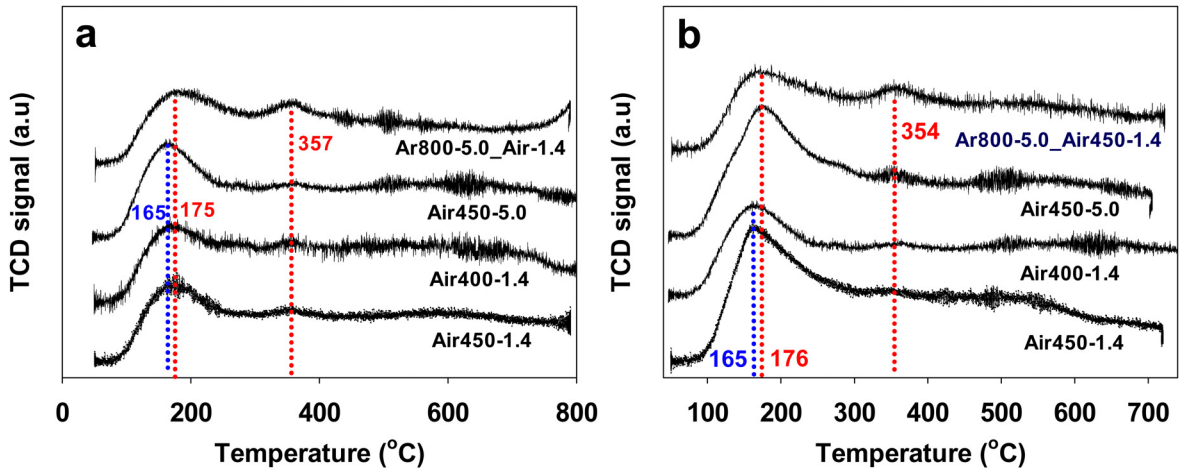

Fig. 4 NH_3-TPD profiles (a), and CO_2-TPD profiles (b) of CeO_2 samples calcined under various conditions.

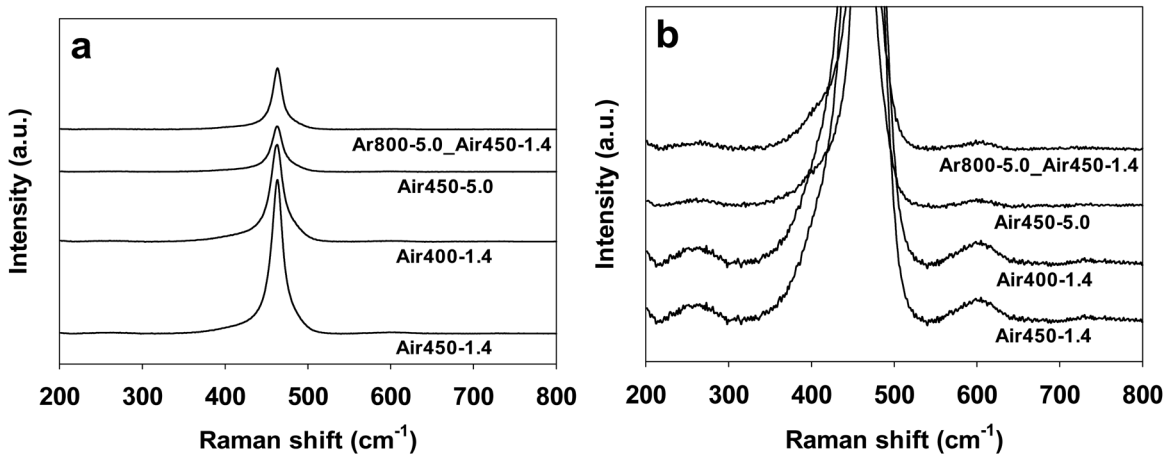

Fig. 5 Raman spectra of CeO_2 samples calcined under various conditions. (b) is the zoom-in image of (a).

are listed in Table 1. The CeO_2 samples calcined in air at 450 °C exhibit close $I_D/I_{F_{2g}}$ values of 0.0080–0.0086 regardless of one or two steps, while the sample calcined in air at 400 °C by one step shows a lower $I_D/I_{F_{2g}}$ value of 0.0073. These results suggest that a higher calcination temperature (in air) results in a larger amount of defects.

The XPS spectra of CeO_2 samples calcined under various conditions are presented in Fig. 6. 8 Ten peaks can be deconvoluted for the Ce 3d spectra, *i.e.*, μ_0 (885.6 eV), μ_1 (881.4 eV), μ_0' (903.5 eV), μ_1' (899.2 eV), ν_0 (882.6 eV), ν_1 (888.9 eV), ν_2 (898.3 eV), ν_0' (900.9 eV), ν_1' (907.5 eV), and ν_2' (916.7 eV), corresponding to the spin–orbit splitting of Ce $3d_{5/2}$ (μ_0, μ_1, ν_0, ν_1, and ν_2) and Ce $3d_{3/2}$ (μ_0', μ_1', ν_0', ν_1', and ν_2').[59,73,74] The concentration of Ce^{3+} (Ce^{3+} %) is calculated from the ratio of peak areas of Ce^{3+} (μ_0, μ_1, μ_0', and μ_1') to the peak areas of Ce^{3+} and Ce^{4+} (ν_0, ν_1, ν_2, ν_0', ν_1', and ν_2') based on the equation below:

$$Ce^{3+}\% = \frac{\text{Peak area of } Ce^{3+}}{\text{Peak area of } (Ce^{3+} + Ce^{4+})} \times 100$$

The calculated Ce^{3+}% values are listed in Table 1. They are in the range of 24.6–25.9%, showing that the different calcination conditions have no significant effect on the Ce^{3+}% values of the resulting CeO_2 samples.

Regarding the O 1s XPS spectra, three peaks corresponding to the lattice oxygen (O_L), the oxygen related to vacancy (O_V), the chemisorbed oxygen (O_C) can be deconvoluted at *ca.* 529.4 eV, 531.5 eV, and 533.5 eV, respectively.[16,19] The concentration of surface oxygen vacancies is calculated from the ratio of peak areas of O_V to peak areas of O_L, O_V and O_C based on the equation below:

$$O_V\% = \frac{\text{Peak area of } O_V}{\text{Peak area of } (O_L + O_V + O_C)} \times 100$$

The calculated O_V% values are listed in Table 1. The two-step calcined sample Ar800-5.0_Air-1.4 exhibits the highest O_V% value of 38%, followed by Air450-1.4 (31.6%), and the samples Air400-1.4 and Air450-5.0 show O_V% values of 28.6% and 28.2%, respectively. These results suggest that the first

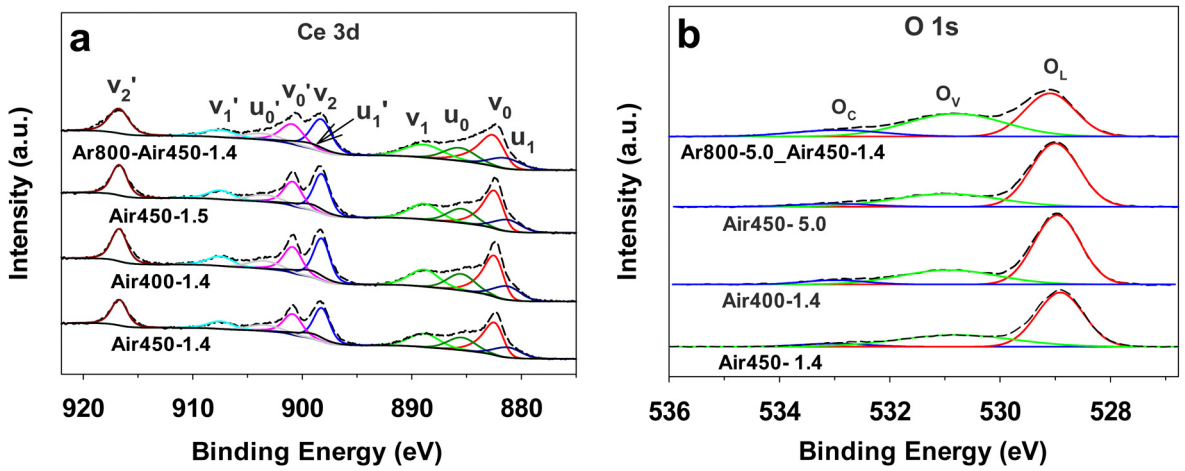

Fig. 6 Ce 3d XPS spectra (a) and O 1s XPS spectra (b) of CeO_2 samples calcined under various conditions.

calcination step (at 800 °C in argon for 3 h) enhances the formation of oxygen vacancies. In addition, the XPS Ce^{3+}% values do not correlate with the XPS O_V% values of these CeO_2 samples. A possible reason could be that not all the oxygen vacancies are correlated with the presence of Ce^{3+}, because Frenkel-type oxygen vacancies can be formed due to the presence of interstitial oxygen ions.[70,75] A study on CeO_2 (obtained by calcination of cerium acetate at 600 °C) by pulsed neutron diffraction experiments has demonstrated the presence of Frenkel-type oxygen defects, which consist of interstitial oxygen ions and corresponding oxygen vacancies.[75] Moreover, according to Table 1, the Raman peak density ratios, $I_D/I_{F_{2g}}$ values, do not correspond to the XPS Ce^{3+}% values or the XPS O_V% values. A possible reason could be that the defects measured by Raman do not solely originate from the presence of Ce^{3+} or oxygen vacancy, and as mentioned above, the F_{2g} peak is sensitive to any disorder including oxygen vacancies, interstitial oxygen defects, dislocation, grain boundaries, *etc.*[72,76,77]

3.4. Catalytic activity

The catalytic activity of the CeO_2 samples for the direct conversion of CO_2 into DMC was evaluated by the DMC formation rate. For easy comparison, the data of a CeO_2 sample without pores[15] and a commercially available CeO_2 sample (Strem Chemicals) with a lower BET surface area measured in this study are also included in Table 1. According to Table 1, all the one-step calcined CeO_2 samples exhibit a much higher DMC formation rate (8.4–14.8 mmol g^{-1} h^{-1}) than the two-step calcined CeO_2 sample Ar800-5.0_Air-1.4 (3.3 mmol g^{-1} h^{-1}), and higher than the nonporous CeO_2 and the commercial CeO_2. Given that all the samples exhibit a close Ce^{3+} concentration of 24.6–25.9%, the higher DMC formation rates of the one-step calcined samples could be due to the following reasons: the amounts of both the weak basicity and weak acidity, the CO_2 uptake at room temperature, and the BET surface area of the one-step calcined catalysts are all higher than that of the two-step calcined sample, as these parameters have been reported to facilitate DMC formation.[11,19,33,47,55,56,69] Regarding the oxygen vacancy concentration (O_V%), although it is expected to improve DMC formation,[16,19,21,30,46,57,58] there is a suggestion that areas with high oxygen vacancies where some of the carbonates can be trapped will activate the internal bonds in undesired manners, which would make the enrichment of more oxygen vacancies less efficient in DMC formation.[78] Indeed, the two-step calcined sample has the highest O_V% but does not show the highest DMC formation rate in this study, which is in good agreement with the previous report.[69]

Among the three one-step calcined samples, the one (Air450-1.4) obtained with a heating rate of 1.4 °C min^{-1} at 450 °C shows the highest DMC formation rate of 14.8 mmol g^{-1} h^{-1}. The data in Table 1 show that both the calcination temperature and the heating rate hugely affect the properties of the resulting CeO_2, consequently affecting the catalytic performance, which is in good agreement with a previous report that the heating rate plays an important role in determining the properties of porous materials.[79] The sample Air450-1.4 prepared by calcination at 450 °C with a ramp rate of 1.4 °C min^{-1} shows the highest DMC formation rate could be due to the reason that it exhibits the optimum combination of the parameters affecting the catalytic performance. As shown in Table 1, this sample shows the highest CO_2 uptake at room temperature and the highest XPS O_V% (yet lower than that of the two-step calcined sample) among the three samples, and moderate weak acidity and weak basicity. As all these parameters have been reported to play a role in the catalytic activity, it seems that the catalytic performance is a result of the superimposition of these factors. This is in good agreement with the claim made by Tomishige *et al.* that it is difficult to elucidate the crucial factors that can influence the catalytic activity of CeO_2 catalysts towards DMC formation from CO_2 and methanol.[17]

To further analyse the effect of the physicochemical properties of the CeO_2 samples on the DMC formation rate of all the samples, the correlation between the DMC formation rates and various parameters is presented in Fig. 7. It can be seen that the DMC formation rate shows a positive correlation between the

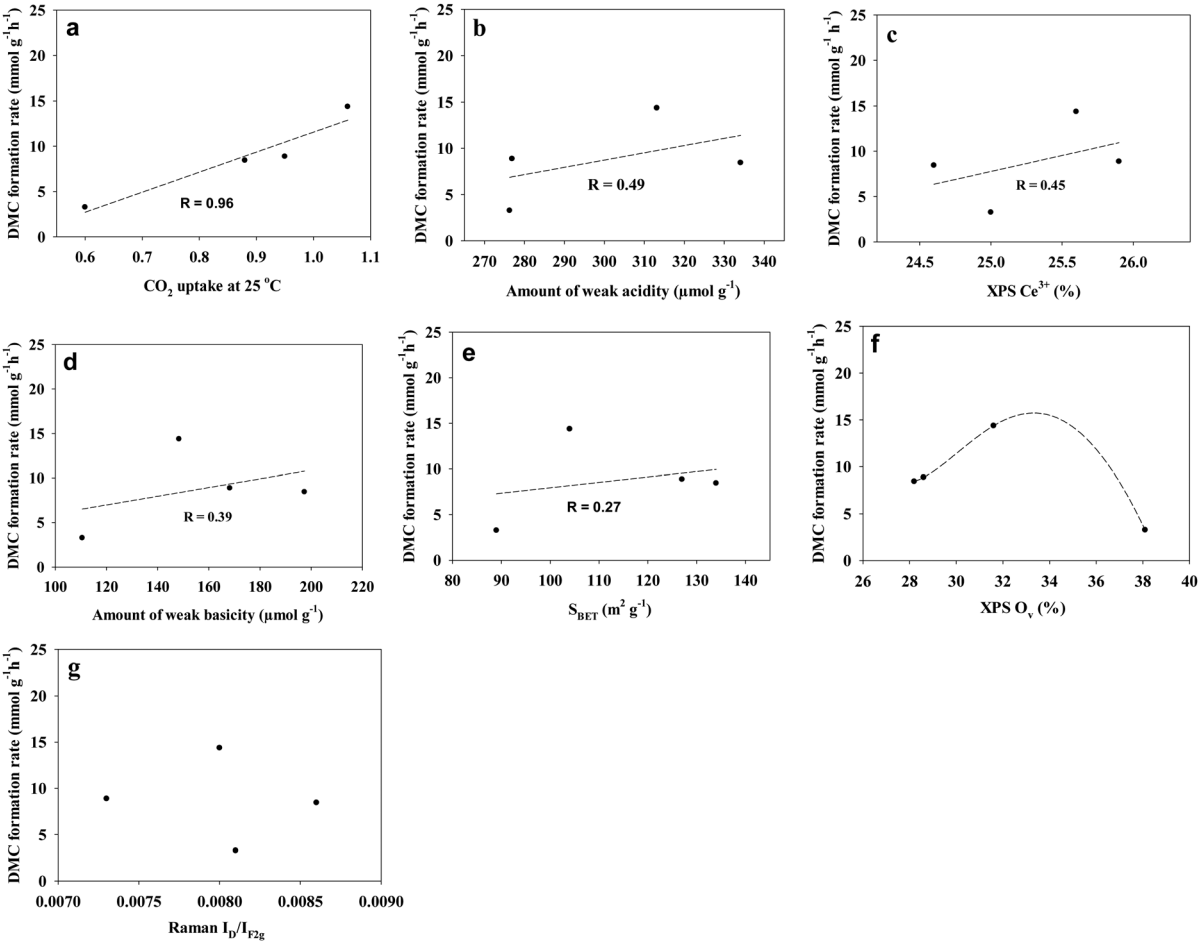

Fig. 7 Effect of various parameters of CeO_2 samples on the DMC formation rate: (a) CO_2 uptake at 25 °C, (b) amount of weak acidity (NH_3 uptake at 100–300 °C), (c) XPS Ce^{3+}%, (d) amount of weak basicity (CO_2 uptake at 100–300 °C), (e) BET surface area (S_{BET}), and (f) XPS O_V%, and (g) Raman peak intensity ratio $I_D/I_{F_{2g}}$.

parameters following the order (based on the correlation coefficient R): the CO_2 uptake amount at 25 °C (R = 0.96), the weak acidity (R = 0.49), the Ce^{3+} concentration (R = 0.45), the weak basicity (R = 0.39), and the BET surface area (R = 0.27) of the CeO_2 samples. In addition, Fig. 7f suggests that there seems to be an optimum oxygen vacancy concentration for DMC formation. This is in agreement with previous reports that although the oxygen vacancy is thought to improve the DMC formation, areas with high oxygen vacancies where some of the carbonates can be trapped will activate the internal bonds in an undesired manner, which would make the enrichment of more oxygen vacancies less efficient in DMC formation[69,78] In addition, Fig. 7g shows that there is no correlation between the DMC formation rate and the Raman peak intensity ratio $I_D/I_{F_{2g}}$ of the CeO_2 catalysts in this study. This could be due to the fact that the Raman F_{2g} peak is sensitive to any disorder including oxygen vacancies, interstitial oxygen defects, dislocation, grain boundaries, *etc.*[72,76,77] while not all the defects contribute to the catalytic performance.

For easy comparison, Table 2 lists the CeO_2 catalysts reported in the literature and those developed in this study, along with their preparation processes and their DMC formation rates measured under various conditions. Based on Table 2, the formation rate of 14.8 mmol g^{-1} h^{-1} is much higher than the values of most reported CeO_2 samples that were prepared by a more complex hydrothermal process at 100–120 °C (5.46–8.03 mmol g^{-1} h^{-1})[15,16,80] or reflux processes at 95 °C (5.97 mmol g^{-1} h^{-1})[41] followed by calcination at 500–650 °C, although lower than the value of the samples (17.7–18.2 mmol g^{-1} h^{-1}) that were prepared by the reflux process at 140 °C and calcination at 600 °C[19] or by the reflux process at 100 °C and calcination at 400 °C followed by extra H_2 heat treatment at 400 °C.[69] These results demonstrate that the relatively simple preparation process at a lower temperature (450 °C) developed in this study is a promising approach to preparing highly active CeO_2 catalysts for the direct conversion of CO_2 and methanol to DMC.

The CeO_2 sample with the highest DMC formation rate in this study, *i.e.*, Air450-1.4, was further studied by *in situ* diffuse reflectance infrared Fourier transform spectroscopy. *In situ* DRIFTS measurement was carried out by pre-adsorption of methanol followed by purging CO_2 at 140 °C, and the spectra

Table 2 Comparison of CeO_2 catalysts prepared by different processes and their catalytic performance in converting CO_2 into DMC

Catalyst	Preparation process	DMC formation rate (mmol g^{-1} h^{-1})	Reaction conditions	Ref.
CeO_2 (Air450-1.4)	Mixing at room temperature + drying at 70 °C and 100 °C + calcination at 450 °C	14.8	140 °C, 5 MPa, 3 h	This work
CeO_2	Calcination of commercial CeO_2 at 600 °C	11	130 °C, 0.2 mol CO_2, 2 h	11
CeO_2 spindles	Refluxing at 95 °C + calcination at 650 °C + chemical redox etching	5.97	140 °C, 4.5 MPa, 3 h	41
CeO_2 nanowires	Solvothermal at 140 °C + H_2 heat treatment at 500 °C	3.37	120 °C, 5 MPa, 5 h	46
CeO_2 rods	Refluxing at 140 °C + calcination at 600 °C	17.7 ± 2.3	140 °C, 5 MPa, 3 h	19
CeO_2	Refluxing at 100 °C + calcination at 400 °C + H_2 heat treatment at 400 °C	18.22 ± 0.64	140 °C, 5 MPa, 3 h	69
CeO_2	Hydrothermal at100 °C + calcination at 600 °C	5.46	140 °C, 6.8 MPa, 2 h	16
CeO_2 spindles	Hydrothermal at 120 °C + calcination at 600 °C	8.03	140 °C, 5 MPa, 2 h	15
CeO_2 quantum dots	Hydrothermal at 150 °C	2.03	140 °C, 5 MPa, 2 h	80
CeO_2	Co-precipitation method + calcination at 600 °C	0.51	120 °C, 15 MPa, 4 h	33
CeO_2	Precipitation + salcination at 550 °C	2.26	140 °C, 3 MPa, 4 h	32

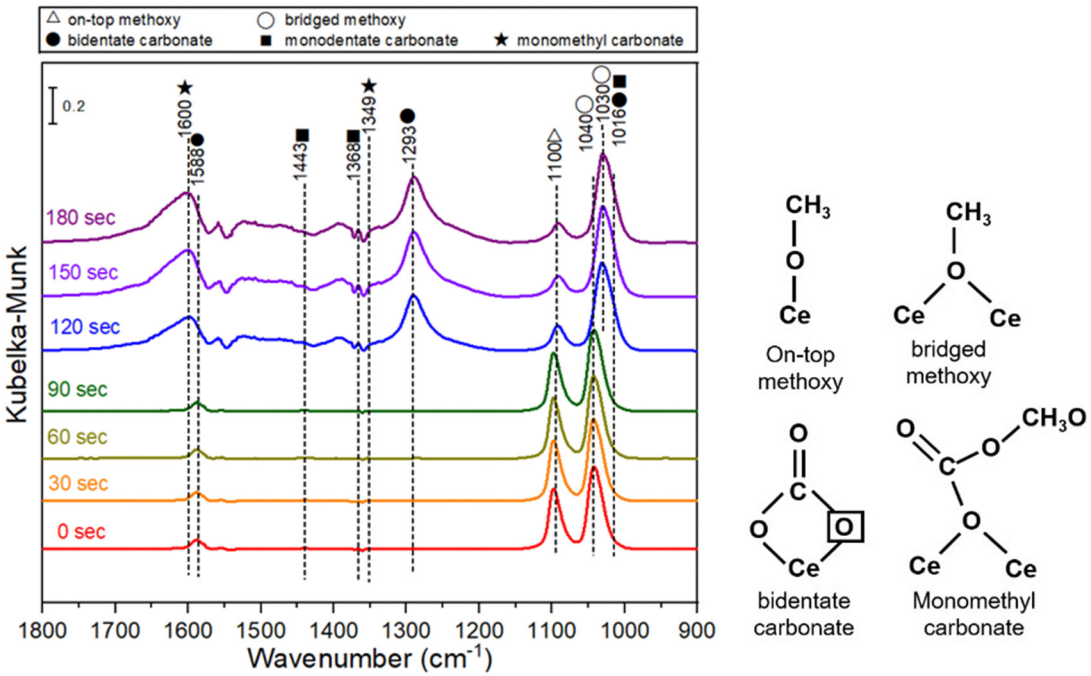

Fig. 8 *In situ* DRIFTS spectra of CeO_2 (Air450-1.4) with pre-adsorbed methanol followed by purging CO_2 at 140 °C.

are shown in Fig. 8. Bands at 1588, 1293 and 1016 cm^{-1} are ascribed to bidentate carbonate. Bands at 1040 and 1030 cm^{-1} are assigned to bridged methoxy groups and bands at 1100 cm^{-1} are on-top methoxy species. Bands at 1600 and 1349 cm^{-1} are due to monomethyl carbonate and bands at 1443, 1368 and 1016 cm^{-1} are corresponding to monodentate carbonate.[19,81] According to the spectra in Fig. 8, it is expected that the methanol adsorption on the CeO_2 catalyst leads to the formation of on-top methoxy species, while the CO_2 adsorption on the CeO_2 catalyst results in the formation of bidentate carbonate. The decrease of the on-top methoxy species is accompanied by the appearance of monomethyl carbonate, which suggests that monomethyl carbonate is formed due to the reaction between the on-top methoxy and the bidentate carbonate, and DMC is formed due to the reaction of the monomethyl carbonate and another on-top methoxy species. This is in good agreement with the reported DMC formation mechanism.[19,82]

4. Conclusions

Porous CeO_2 was prepared by a simple method, in which the raw materials were mixed at room temperature and then dried at 70 °C and 100 °C consecutively, followed by calcination at 400 or 450 °C with a heating rate of 1.4 or 5.0 °C min^{-1}. Calcination at 450 °C with a heating rate of 1.4 °C min^{-1} results in CeO_2 showing the highest DMC formation rate of 14.8 mmol g^{-1} h^{-1}, which is much higher than that of the majority of the reported CeO_2 catalysts that were prepared by a

more complex hydrothermal process at 100–120 °C (5.46–8.03 mmol g^{-1} h^{-1}) or reflux processes at 95 °C (5.97 mmol g^{-1} h^{-1}) followed by calcination at 500–650 °C. Further study shows that the DMC formation rate has a positive link to the parameters following the order (based on the correlation coefficient R): the CO_2 uptake amount at 25 °C (R = 0.96), the weak acidity (R = 0.49), the Ce^{3+} concentration (R = 0.45), the weak basicity (R = 0.39), and the BET surface area (R = 0.27) of the CeO_2 catalysts. In addition, there seems to be an optimum oxygen vacancy concentration for the DMC formation rate, while no correlation is found between the DMC formation rate and the Raman peak intensity ratio $I_D/I_{F_{2g}}$ of the CeO_2 catalysts in this study. The *in situ* DRIFTS measurement suggests that monomethyl carbonate is formed due to the reaction between the on-top methoxy and the bidentate carbonate, and DMC is formed due to the reaction of the monomethyl carbonate and another on-top methoxy species. This study provides a simple and easy-to-scale-up strategy for the preparation of a porous CeO_2 catalyst for the direct conversion of CO_2 and methanol to DMC at a lower temperature (450 °C), which could be potentially applicable to other reactions (*e.g.*, the synthesis of diethyl carbonate).

Author contributions

Zhuxian Yang: investigation, methodology, data curation, and writing – original draft. Justin Tay Zheng: data curation, validation, and writing – review & editing. Xinhuan Lu: methodology, data curation, and validation. Monica Mengdie Lin: investigation, validation, and data curation. Dongming Cai: investigation, validation, and data curation. Yankun Wang: investigation and data curation. Wen-Yueh Yu: supervision, methodology, validation, and writing – review & editing. Yanqiu Zhu: supervision, and writing – review & editing. Yongde Xia: supervision, conceptualization, methodology, validation, and writing – review & editing.

Data availability

The data supporting this article have been included as part of the ESI.†

Conflicts of interest

The authors declare that they have no known competing financial interests or personal relationships that could have appeared to influence the work reported in this manuscript.

Acknowledgements

This work was supported by the Leverhulme Trust (RPG-2018–320), the Royal Society (IEC\NSFC\201121), and the National Science and Technology Council (NSTC), Taiwan (110-2221-E-002-012-MY3 and 112-2221-E-002-041-MY3).

References

1 G. Fiorani, A. Perosa and M. Selva, *Green Chem.*, 2018, **20**, 288–322.
2 Y. Ono, *Appl. Catal., A*, 1997, **155**, 133–166.
3 M. A. Pacheco and C. L. Marshall, *Energy Fuels*, 1997, **11**, 2–29.
4 P. Kumar, V. C. Srivastava, U. L. Stangar, B. Music, I. M. Mishra and Y. Z. Meng, *Catal. Rev.*, 2021, **63**, 363–421.
5 F. Y. Tu, H. J. Lai, T. A. Chiu, J. C. Jiang and W. Y. Yu, *Surf. Interfaces*, 2023, **43**, 103597.
6 D. C. Shi, S. Heyte, M. Capron and S. Paul, *Green Chem.*, 2022, **24**, 1067–1089.
7 M. J. Schneider, M. Haumann, M. Stricker, J. Sundermeyer and P. Wasserscheid, *J. Catal.*, 2014, **309**, 71–78.
8 H. Z. Tan, Z. Q. Wang, Z. N. Xu, J. Sun, Z. N. Chen, Q. S. Chen, Y. M. Chen and G. C. Guo, *Catal. Sci. Technol.*, 2017, **7**, 3785–3790.
9 L. G. Wang, Y. Wang, S. M. Liu, L. J. Lu, X. Y. Ma and Y. Q. Deng, *Catal. Commun.*, 2011, **16**, 45–49.
10 Z. Q. Hou, L. G. Luo, K. Liu, C. Z. Liu, Y. Y. Wang and L. Y. Dai, *Chem. Eng. J.*, 2014, **236**, 415–418.
11 Y. Yoshida, Y. Arai, S. Kado, K. Kunimori and K. Tomishige, *Catal. Today*, 2006, **115**, 95–101.
12 S. S. Peng, X. B. Shao, M. X. Gu, G. S. Zhang, C. Gu, Y. Nian, Y. M. Jia, Y. Han, X. Q. Liu and L. B. Sun, *Angew. Chem., Int. Ed.*, 2022, **61**, e202215157.
13 H. Babad and A. G. Zeiler, *Chem. Rev.*, 1973, **73**, 75–91.
14 H. J. Lee, W. Joe and I. K. Song, *Korean J. Chem. Eng.*, 2012, **29**, 317–322.
15 S. P. Wang, L. F. Zhao, W. Wang, Y. J. Zhao, G. L. Zhang, X. B. Ma and J. L. Gong, *Nanoscale*, 2013, **5**, 5582–5588.
16 B. Liu, C. M. Li, G. Q. Zhang, X. S. Yao, S. S. C. Chuang and Z. Li, *ACS Catal.*, 2018, **8**, 10446–10456.
17 K. Tomishige, Y. Gu, T. Chang, M. Tamura and Y. Nakagawa, *Mater. Today Sustain.*, 2020, **9**, 100035.
18 C. Daniel, Y. Schuurman and D. Farrusseng, *J. Catal.*, 2021, **394**, 486–494.
19 W. F. Kuan, W. Y. Yu, F. Y. Tu, C. H. Chung, Y. C. Chang, M. M. Lin, T. H. Yu and L. J. Chen, *Chem. Eng. J.*, 2022, **430**, 132941.
20 G. L. Yang, A. Z. Jia, J. D. Li, F. Li and Y. J. Wang, *Mol. Catal.*, 2022, **528**, 112471.
21 W. F. Kuan, C. H. Chung, M. M. Lin, F. Y. Tu, Y. H. Chen and W. Y. Yu, *Mater. Today Sustain.*, 2023, **23**, 100425.
22 B. Peng, H. R. Dou, H. Shi, E. E. Ember and J. A. Lercher, *Catal. Lett.*, 2018, **148**, 1914–1919.
23 W. Donphai, O. Phichairatanaphong, R. Fujii, P. Li, T. Chang, M. Yabushita, Y. Nakagawa and K. Tomishige, *Mater. Today Sustain.*, 2023, **24**, 100549.
24 D. Stoian, F. Medina and A. Urakawa, *ACS Catal.*, 2018, **8**, 3181–3193.
25 K. Tomishige and K. Kunimori, *Appl. Catal., A*, 2002, **237**, 103–109.
26 D. J. Faria, L. M. dos Santos, F. L. Bernard, I. S. Pinto, M. Resende and S. Einloft, *RSC Adv.*, 2020, **10**, 34895–34902.

27 J. C. Choi, L. N. He, H. Yasuda and T. Sakakura, *Green Chem.*, 2002, **4**, 230–234.
28 Z. F. Zhang, Z. W. Liu, J. A. Lu and Z. T. Lie, *Ind. Eng. Chem. Res.*, 2011, **50**, 1981–1988.
29 N. Wang, Y. Liu, A. Huang and J. Caro, *Microporous Mesoporous Mater.*, 2015, **207**, 33–38.
30 G. L. Yang, H. B. Wang, A. Z. Jia, J. D. Li and Y. J. Wang, *New J. Chem.*, 2023, **47**, 12477–12486.
31 W. Sun, P. L. Li, M. Yabushita, Y. Nakagawa, Y. Q. Wang, A. Nakayama and K. Tomishige, *ChemSusChem*, 2023, **16**, e202300768.
32 G. Q. Zhang, Y. Zhou, Y. L. Yang, T. T. Kong, Y. Song, S. Zhang and H. Y. Zheng, *Molecules*, 2023, **28**, 3785.
33 P. Kumar, P. With, V. C. Srivastava, R. Glaser and I. M. Mishra, *J. Environ. Chem. Eng.*, 2015, **3**, 2943–2947.
34 K. Tomishige, T. Sakaihori, Y. Ikeda and K. Fujimoto, *Catal. Lett.*, 1999, **58**, 225–229.
35 K. T. Jung and A. T. Bell, *J. Catal.*, 2001, **204**, 339–347.
36 C. J. Jiang, Y. H. Guo, C. G. Wang, C. W. Hu, Y. Wu and E. B. Wang, *Appl. Catal., A*, 2003, **256**, 203–212.
37 Q. X. Zheng, R. Nishimura, Y. Sato, H. Inomata, M. Ota, M. Watanabe and S. Camy, *Chem. Eng. J.*, 2022, **429**, 132378.
38 X. L. Wu, M. Xiao, Y. Z. Meng and Y. X. Lu, *J. Mol. Catal. A: Chem.*, 2005, **238**, 158–162.
39 W. Sun, L. Zheng, Y. Q. Wang, D. D. Li, Z. R. Liu, L. Wu, T. Fang and J. Q. Wu, *Ind. Eng. Chem. Res.*, 2020, **59**, 4281–4290.
40 A. H. Tamboli, N. Suzuki, C. Terashima, S. Gosavi, H. Kim and A. Fujishima, *Catalysts*, 2021, **11**, 223.
41 T. Kulthananat, P. Kim-Lohsoontorn and P. Seeharaj, *Ultrason. Sonochem.*, 2022, **90**, 106164.
42 Y. Z. Wang, S. Geng, F. Liu, M. Q. Yao, J. Ma, J. X. Cao and Z. W. Li, *J. Colloid Interface Sci.*, 2023, **652**, 1984–1993.
43 C. M. Marin, L. Li, A. Bhalkikar, J. E. Doyle, X. C. Zeng and C. L. Cheung, *J. Catal.*, 2016, **340**, 295–301.
44 S. Y. Zhao, S. P. Wang, Y. J. Zhao and X. B. Ma, *Chin. Chem. Lett.*, 2017, **28**, 65–69.
45 P. Kumar, L. Matoh, R. Kaur and U. L. Stangar, *Fuel*, 2021, **285**, 119083.
46 Z. W. Fu, Y. H. Yu, Z. Li, D. M. Han, S. J. Wang, M. Xiao and Y. Z. Meng, *Catalysts*, 2018, **8**, 164.
47 E. Leino, N. Kumar, P. Maki-Arvela, A. Aho, K. Kordas, A. R. Leino, A. Shchukarev, D. Y. Murzin and J. P. Mikkola, *Mater. Chem. Phys.*, 2013, **143**, 65–75.
48 M. Zhang, M. Xiao, S. J. Wang, D. M. Han, Y. X. Lu and Y. Z. Meng, *J. Cleaner Prod.*, 2015, **103**, 847–853.
49 J. Y. Zhang, S. Y. Zhao, Y. J. Zhao, X. B. Ma and S. P. Wang, *Asia-Pac. J. Chem. Eng.*, 2021, **16**, e2517.
50 P. Kumar, P. With, V. C. Srivastava, K. Shukla, R. Glaser and I. M. Mishra, *RSC Adv.*, 2016, **6**, 110235–110246.
51 S. P. Wang, J. J. Zhou, S. Y. Zhao, Y. J. Zhao and X. B. Ma, *Chin. Chem. Lett.*, 2015, **26**, 1096–1100.
52 P. Unnikrishnan and S. Darbha, *J. Chem. Sci.*, 2016, **128**, 957–965.
53 B. Liu, C. M. Li, G. Q. Zhang, L. F. Yan and Z. Li, *New J. Chem.*, 2017, **41**, 12231–12240.
54 K. W. La, J. C. Jung, H. Kim, S. H. Baeck and I. K. Song, *J. Mol. Catal. A: Chem.*, 2007, **269**, 41–45.
55 H. J. Lee, S. Park, I. K. Song and J. C. Jung, *Catal. Lett.*, 2011, **141**, 531–537.
56 H. J. Lee, W. Joe, J. C. Jung and I. K. Song, *Korean J. Chem. Eng.*, 2012, **29**, 1019–1024.
57 S. Wada, K. Oka, K. Watanabe and Y. Izumi, *Front. Chem.*, 2013, **1**, 8.
58 C. H. Chung, F. Y. Tu, T. A. Chiu, T. T. Wu and W. Y. Yu, *Chem. Lett.*, 2021, **50**, 856–865.
59 H. Liu, W. J. Zou, X. L. Xu, X. L. Zhang, Y. Q. Yang, H. J. Yue, Y. Yu, G. Tian and S. H. Feng, *J. CO_2 Util.*, 2017, **17**, 43–49.
60 J. Li, Z. Y. Zhang, Z. M. Tian, X. M. Zhou, Z. P. Zheng, Y. Y. Ma and Y. Q. Qu, *J. Mater. Chem. A*, 2014, **2**, 16459–16466.
61 Q. X. Zhou, S. L. Ma and S. H. Zhan, *Appl. Catal., B*, 2018, **224**, 27–37.
62 S. W. Yang, H. D. Shen, F. Cheng, C. Wu, Y. L. Cao, S. F. Zhuo, Q. Y. Zhang and H. P. Zhang, *J. Mater. Chem. A*, 2020, **8**, 14006–14014.
63 C. M. Ho, J. C. Yu, T. Kwong, A. C. Mak and S. Y. Lai, *Chem. Mater.*, 2005, **17**, 4514–4522.
64 G. N. Li, S. Dissanayake, S. L. Suib and D. E. Resasco, *Appl. Catal., B*, 2020, **267**, 118373.
65 S. K. Lee, C. Jo, J. Kim and R. Ryoo, *Microporous Mesoporous Mater.*, 2020, **293**, 109767.
66 Z. J. Gong, Y. R. Li, H. L. Wu, S. D. Lin and W. Y. Yu, *Appl. Catal., B*, 2020, **265**, 118524.
67 Y. H. Wang, C. H. Chuang, T. A. Chiu, C. W. Kung and W. Y. Yu, *J. Phys. Chem. C*, 2020, **124**, 12521–12530.
68 Z. J. Gong, C. C. Chien, S. Mudhulu, J. C. S. Wu, N. Daneu, M. M. Krzmanc and W. Y. Yu, *J. Catal.*, 2022, **416**, 222–232.
69 Z. Yang, M. M. Lin, X. Lu, J. T. Zheng, W.-Y. Yu, Y. Zhu, H. Chang and Y. Xia, *Chem. Eng. J.*, 2024, **486**, 150339.
70 Z. L. Wu, M. J. Li, J. Howe, H. M. Meyer and S. H. Overbury, *Langmuir*, 2010, **26**, 16595–16606.
71 T. Taniguchi, T. Watanabe, N. Sugiyama, A. K. Subramani, H. Wagata, N. Matsushita and M. Yoshimura, *J. Phys. Chem. C*, 2009, **113**, 19789–19793.
72 C. M. Yang, Y. X. Lu, L. Zhang, Z. J. Kong, T. Y. Yang, L. Tao, Y. Q. Zou and S. Y. Wang, *Small Struct.*, 2021, **2**, 2100058.
73 R. H. Gao, D. S. Zhang, P. Maitarad, L. Y. Shi, T. Rungrotmongkol, H. R. Li, J. P. Zhang and W. G. Cao, *J. Phys. Chem. C*, 2013, **117**, 10502–10511.
74 F. Larachi, J. Pierre, A. Adnot and A. Bernis, *Appl. Surf. Sci.*, 2002, **195**, 236–250.
75 E. Mamontov and T. Egami, *J. Phys. Chem. Solids*, 2000, **61**, 1345–1356.
76 B. Feng, H. Hojo, T. Mizoguchi, H. Ohta, S. D. Findlay, Y. Sato, N. Shibata, T. Yamamoto and Y. Ikuhara, *Appl. Phys. Lett.*, 2012, **100**, 073109.
77 H. Hojo, E. Tochigi, T. Mizoguchi, H. Ohta, N. Shibata, B. Feng and Y. Ikuhara, *Appl. Phys. Lett.*, 2011, **98**, 153104.
78 M. Capdevila-Cortada, G. Vilé, D. Teschner, J. Pérez-Ramírez and N. López, *Appl. Catal., B*, 2016, **197**, 299–312.

79 Z. X. Yang and R. Mokaya, *Microporous Mesoporous Mater.*, 2008, **113**, 378–384.
80 Z. Q. Wang, M. J. Zhang, X. B. Hu, V. P. Dravid, Z. N. Xu and G. C. Guo, *Chem. Commun.*, 2020, **56**, 403–406.
81 S. Rousseau, O. Marie, P. Bazin, M. Daturi, S. Verdier and V. Harle, *J. Am. Chem. Soc.*, 2010, **132**, 10832–10841.
82 M. Honda, M. Tamura, Y. Nakagawa, K. Nakao, K. Suzuki and K. Tomishige, *J. Catal.*, 2014, **318**, 95–107.